DOI: 10.13009/EUCASS2025-134
11TH EUROPEAN CONFERENCE FOR AERONAUTICS AND SPACE SCIENCES (EUCASS)

BATTERY PACK THERMAL BEHAVIOUR MODELLING FOR ELECTRIC AIRCRAFT

*Tristan Bakker**†, Wim Lammen* and Fabrizio Oliviero*+
* Collaborative Engineering Systems department, NLR – Royal Netherlands Aerospace Centre
Anthony Fokkerweg 2, 1059 CM Amsterdam
+ Flight Performance & Propulsion Group, Delft University of Technology
Kluyverweg 1, 2629 HS Delft

Tristan.bakker@nlr.nl – wim.lammen@nlr.nl – F.Oliviero@tudelft.nl
† Corresponding Author

Abstract

The call for net-zero emission flights by 2050 is prompting the design of alternative aircraft propulsion systems. In this framework, the electrification of both propulsive and non-propulsive loads onboard aircraft is thoroughly investigated. Despite the large number of battery electric (BE) aircraft concepts , the only certified BE aircraft is the two-seater Pipistrel Velis Electro. In this study, the mission performance and thermal stability of the battery packs of the Velis Electro are analyzed by means of simulation, using a combination of electric equivalent circuit models (EECM) and lumped parameter thermal network (LPTN) models. The models were validated with data from NLR's Velis Electro aircraft where a maximum prediction error below 2% was found for both voltage and temperature.

1 Introduction

Since the first human flight in 1903, aviation has encountered a fast growth becoming an integral part of our society for both human and goods transportation. Despite the technological advancements along these years, one constant has remained the use of fossil fuels-based propulsion systems. Nowadays, engines are highly efficient, however, due to the increased number of flights it is forecasted that greenhouse gas emissions from aviation could increase by a factor of 3.6 by 2050, if no action is taken [1]. To meet the Paris Agreement goal of net-zero emissions aviation by 2050 [2], a radical change of the current powertrain designs is needed. Alternative propulsion systems, i.e., fuel cells, batteries, hybrid-systems, are investigated as potential alternatives for future aircraft.

The battery electric (BE) aircraft concept foresees the use of batteries for both non-propulsive and propulsive power. Several BE propulsion concepts have been studied [2], [3], [4], but there are still many open challenges, i.e., battery mass and volume, safety issues, performance degradation, and operational constraints. These challenges have hindered the development of BE aircraft, with only one certified BE aircraft available on the market today: the Pipistrel Velis Electro[5]. This study aims to address the challenge of thermal stability in BE aircraft by evaluating mission performance and thermal stability of batteries. This will require a coupling to be made between an electrical model, modelling the electrical performance in terms of current, voltage, state-of-charge and heat generation and a thermal model, modelling the temperature evolution of the battery pack.

When attempting to model the electrical performance of a lithium-ion battery pack it is important to first model the individual battery cells making up the battery pack. The modelling approaches available for modelling the electrical performance of lithium-ion battery cells are detailed-electrochemical models, electric equivalent circuit models and data-driven models. In [6], [7], [8] coupled electrical-thermal models have been developed using detailed electrochemical models like the Doyle-Fuller-Newman (DFN) model [9] and derivates of this model like the single particle model (SPM) [10], [11], [12]. Accurate modelling results were achieved with this modelling approach in [6], [7], [8]. However, the electrochemical-models require a large amount of parameters to be estimated or known a-priori and are generally best suited for detailed simulation of single lithium-ion battery cells as the complexity and computational cost of these models is high[13], [14].

On the other end of the spectrum are the data-driven models. These models use machine learning techniques to learn the relationships between input and output variables [15]. In [15], [16], data driven approaches where used to model

DOI: 10.13009/EUCASS2025-134

the voltage behaviour of lithium ion battery cells. Both studies achieved accurate modelling results with the data driven approaches. However they required large amounts of experimental data to be available to train the models. Since the models are developed solely based on measured data and with minimum to zero use of the battery physics, they are less effective in describing internal physicochemical phenomena [14].
Another option for modelling the electrical behaviour of lithium ion-battery cells is with the use of electric equivalent circuit models (EECM). EECMs simulate the causality between the battery current and the voltage by constructing an electric circuit using resistors and capacitors, although they do not inherently represent the physical effects [14]. EECMs have been used in [19], [20] to simulate the electric behaviour of lithium ion batteries with great success. In [20], [21], [22] comparisons are made between different types of EECMs and the modelling accuracy. From these studies it could be concluded that by adding more circuit parameters to the model, more complex battery behaviour could be modelled with the risk of overfitting the data. Similar to data-driven models, EECMs require experimental data to allow for model parameter estimation. Approaches for this parameter estimation have been described in [23], [24]. The EECM approach strikes a good balance between model complexity and computational costs when compared to the electrochemical and data driven approaches. For this reason the EECM is the electrical model of choice in this work.
The thermal part of the developed model should be able to calculate the temperature evolution of the battery pack based on the heat generation rate. Various approaches can be taken for this battery thermal modelling. These mainly include physical modelling techniques [25], [26], [27] or lumped thermal models [28], [29], [30]. Physical modelling techniques such as Finite Element Modelling (FEM), Finite Volume Modelling (FVM) or general partial differential equations (PDE) have been successfully used in [31], [32], [33] to get the three-dimensional (3D) temperature distribution of battery cells. These models however required high computational cost [34] making them ill-suited for simulation of an entire battery pack. Lumped parameter thermal network (LPTN) models have been widely used to evaluate battery temperature behaviour. The method is straightforward to implement and suited for real time applications [34]. In [30], [35] the LPTN was successfully used to estimate the battery core temperature from the surface temperature readings. The work performed in [30], [34], [35] focusses at the modelling of single battery cells inside the pack. The modelling of a full lithium-ion aircraft battery pack with a coupled electro-thermal model is relatively unexplored. This work aims to fill in this gap by developing a coupled electro-thermal model of a battery pack for an aerospace application. The model has been validated using flight data of NLR's Pipistrel Velis Electro aircraft. This aircraft features two 11 kWh battery packs, arranged in parallel for redundancy Figure. 2. Each of the packs contains 1152, 18650 Lithium-ion battery cells arranged in a 96S12P configuration [5]. The battery cells contained in the pack are the INR18650-33G developed by Samsung. This battery cell features a high-capacity nickel-manganese-cobalt (NMC) cathode chemistry and has a nominal capacity of 3150 mAh[36].

Figure 1: Image of the NLR Pipistrel Velis Electro

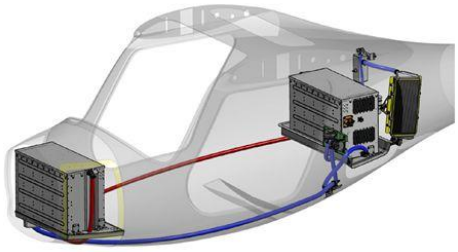

Figure 2: The battery pack in the Pipisrel Velis Electro aircraft[5]

2 Methodology

As discussed in the previous chapter, to model the thermal behaviour of a lithium-ion battery pack, it is necessary to capture both the pack electric characteristics, such as voltage response and state-of-charge evolution, and its thermal characteristics, specifically the pack temperature. This implies that at least two models need to be developed and coupled: one for the electrical behaviour and one for the thermal behaviour.
The primary objective of the electrical model is to simulate the output voltage, change in state-of-charge, and heat generation inside the battery cell based on the current drawn from the cell (positive for charging, negative for discharging) and the cell temperature. The model establishes a relationship between the external characteristics exhibited by the battery during operation and its internal states. A lithium-ion battery model aims to provide accurate relationships between voltage, state-of-charge (SoC), temperature, and state-of-health (SoH). In this work, state-of-charge and state-of-health are defined by equations (2.1) and (2.2) while equation (2.3) describes the relationship between output voltage and battery states. Note that state-of-health is not considered in this work, as it is expected to

DOI: 10.13009/EUCASS2025-134

change only after a large number of flights and thus remain near constant during a single flight. Therefore, state-of-health is treated as a constant during simulation, although its effect can still be accounted for by providing it as an initial condition to the model.

$$SoC = \frac{Q(t)}{Q_{max}} \tag{2.1}$$

$$SoH = \frac{Q_{act}}{Q_{max}^{BOL}} \tag{2.2}$$

$$V(t) = f(SoC(t), I(t), T_c(t)) \tag{2.3}$$

The current drawn from a battery cell is referred to as the current profile, which is a direct input to the model and can be derived from the power required by the electrical load connected to the battery. As discussed in the previous chapter, the EECM approach was chosen for its balance between modelling accuracy, computational cost, and parameter identification precision [20], [21]. The EECM concept will be explained in detail in subsection 2.1.
The EECM uses the battery cell temperature as an additional input, but this requires prior knowledge of the temperature at each timestep. By coupling the electrical model with a thermal model, it becomes possible to simulate the temperature evolution of the battery cell from an initial temperature. The primary goal of the thermal model is to simulate the battery cell temperature based on the heat load generated by the battery (an output from the electrical model), the battery coolant temperature, and the ambient temperature. The modelled battery cell temperature can then serve as an input for the electrical model. A schematic of the coupled electrical and thermal models is shown in Figure 3. In this work, a LPTN model is used as the thermal model, described in more detail in subsection 2.4.

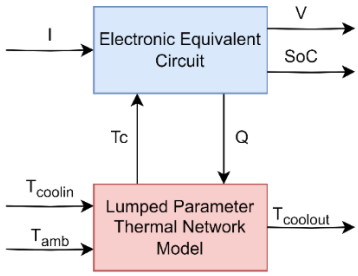

Figure 3: Flowchart illustrating the method used for the electro-thermal model coupling.

2.1 Electric Equivalent Circuit Model

EECMs use a combination of various electrical circuit components such as resistors, capacitors, voltage- and current sources. Different configurations of these components result in different types of EECMs. The most common EECMs are the open circuit voltage model, the Thevenin-circuit model and the Dual polarization model [19]. However, by adding more electric circuit components to these models, other EECMs can be constructed as well.
The parameterization of each of these models starts with finding a relation between the open circuit voltage (OCV) of the battery. This relationship can be found in a constant current discharge curve plot, as seen in Figure 4. From Figure 4 it can clearly be deduced that the OCV increases with temperature [37]. Additionally, the area under each of the plots reduces for lower temperatures indicating a reduction in battery capacity at lower temperatures [37]. This shows the importance of including the battery cell temperature as a model input for the electric model and the need of modelling the evolution of this temperature. With this finding in mind the relationship between OCV, SoC and temperature can be established resulting in the most simple EECM available, the open circuit voltage model as described by equation (2.4).

$$V(t) = V_{OC}(SoC(t), T_c(t)) \tag{2.4}$$

DOI: 10.13009/EUCASS2025-134

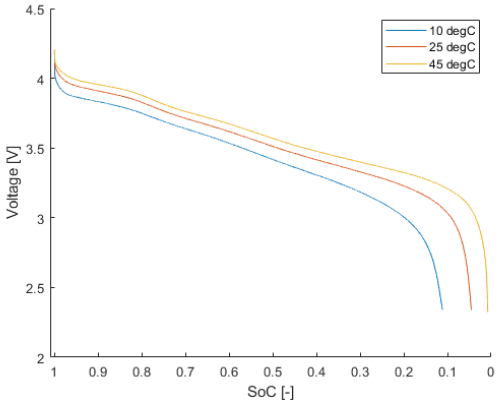

Figure 4: The battery OCV versus SoC for various cell temperatures during a constant 1C discharge

The OCV model is limited as there is no dependency on the current drawn from the battery. This effect can be added to the model by adding a resistor to the open-circuit voltage source [38] as seen in Figure 5. This EECM is called the R_0 or 0-RC EECM. The voltage equation for this model can be seen in equation (2.5). For this model, the internal resistance R_0 can be determined by connecting an electric load to a fully charged battery and detecting both the terminal voltage and the current [19]. Since the load resistance is known, the excess voltage drop compared to the OCV can be attributed to the internal resistance. Ohms law can then be used to determine this internal resistance. In this state the model does not consider the influence of SoC on the value of the R_0 as it is determined only once. If the effect of SoC on R_0 is to be considered, the process of measuring the excess voltage drop compared to the OCV can be repeated at various SoCs. The values of R_0 at the different SoCs can in turn be stored in a lookup table such that the circuit parameter value can be extracted by means of interpolation at the desired SoC. In the same way the dependency of R_0 on T_c can be included in the model. This process of finding the values of electric circuit parameters at different internal battery states requires experimental data. The process on how to obtain the circuit parameters from the experimental data is described in subsection 2.2. The type of experimental data and how this data was obtained will be explained in subsection 2.3.

$$V(t) = V_{oc}\big(SoC(t), T_c(t)\big) - I(t) \cdot R_0(SoC(t), T_c(t)) \tag{2.5}$$

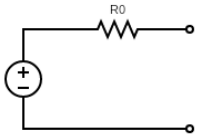

Figure 5: Schematic of 0-RC or R_0 EECM

The 0-RC model can be extended to include the time-dependent dynamics seen in the battery voltage response [19], [20], [21]. This can be achieved by adding one or more resistor-capacitor (RC) pairs to the EECM, yielding an n-RC model, where n represents the number of pairs. Notable examples include the 1-RC and 2-RC EECMs, also known as the Thevenin and Dual Polarization models [22], with the latter providing a more refined representation of polarization characteristics, including concentration and electrochemical polarization [39]. The addition of RC pairs can be extended indefinitely to form n-RC EECMs, with a schematic shown in Figure 6. The resulting cell voltage for the n-RC EECM is determined using equation (2.6), which includes the voltage drop over each RC pair (U_n), calculable using equation (2.7). This equation expresses U_n as a continuous-time function, with τ being the time constant of the RC pair, equal to the product of its resistance and capacitance, both dependent on SoC and T_c (equation (2.8)). To facilitate numerical simulation, equation 2.4 can be rewritten as a discretized ordinary differential equation (ODE), as shown in equation (2.9), where Δt denotes the timestep and j the time instance [22].

$$V(t) = V_{oc}\big(SoC(t), T_c(t)\big) - I(t) \cdot R_0\big(SoC(t), T_c(t)\big) - \sum_{i=1}^{n} U_n(SoC(t), T_c(t), I(t)) \tag{2.6}$$

$$U_n = I \cdot R_n(1 - e^{-\frac{t}{\tau}}) \tag{2.7}$$

DOI: 10.13009/EUCASS2025-134

$$\tau = R_n\big(SoC(t), T_c(t)\big) \cdot C_n(SoC(t), T_c(t)) \tag{2.8}$$

$$U_{n,j+1} = e^{\frac{-\Delta t}{R_n C_n}} \cdot U_{n,j} + R_n \left[1 - e^{\frac{-\Delta t}{R_n C_n}}\right] \cdot I_j \tag{2.9}$$

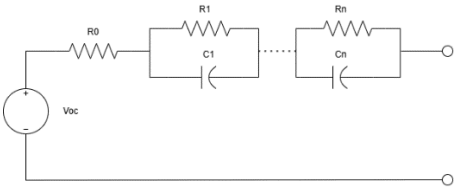

Figure 6: Schematic of n-RC EECM

2.1.1 Heat generation

The heat generation within a lithium-ion battery cell can be attributed to two primary heat sources, as described by equation (2.10): irreversible heat and reversible heat. The irreversible heating, also known as Joule heating, is the dominant heat generation mechanism within the battery cell [40]. This irreversible heating is the heat dissipated through an electric resistor when an electric current flows through it. The heat generation rate caused by this term can be calculated by multiplying the internal resistance of the battery cell by the square of the current as expressed in equation (2.11)or by V_{oc}-*V(t)* when using equation (2.6). Notably, the internal resistance of the battery cell is a function of both the state of charge (SoC) and temperature (T_c), and can be determined by calculating the equivalent electric resistance of all circuit components in the EECM.

$$\dot{Q} = \dot{Q}_{irr} + \dot{Q}_{rev} \tag{2.10}$$

$$\dot{Q}_{irr} = I^2 \cdot R_{internal} \tag{2.11}$$

The reversible heating term arises from the change in entropy of the battery due to the redox reaction, resulting in entropic heat generation. This phenomenon occurs when the lithium content of the electrodes changes, inducing a change in entropy within the materials. As this process is reversible, it is referred to as reversible heating, which can manifest as both positive and negative heat generation, in contrast to irreversible heating, which is always positive [17]. The equation for reversible heat can be derived by rearranging the Gibbs Free Energy equation to Equation 2.12, where *n* represents the number of electrons participating in the redox reaction (equal to 1 for lithium-ion) and *F* denotes the Faraday constant. The entropy change ΔS can be calculated using equation (2.13), allowing equation (2.12) to be simplified to equation (2.14). In Equation (2.14), the factor $\frac{\delta V_{oc}}{\delta T}$ is referred to as the entropic coefficient. Accurate determination of this coefficient is crucial for precise calculation of reversible heat generation. The entropic coefficient indicates the rate of change of the OCV of the battery cell with respect to temperature at a given SoC. This coefficient can be determined experimentally by measuring the change in OCV with respect to temperature at different SoC levels.

$$\dot{Q}_{rev} = -\frac{I}{nF} T \Delta S \tag{2.12}$$

$$\Delta S = nF \frac{\delta V_{oc}}{\delta T} \tag{2.13}$$

$$\dot{Q}_{rev} = -IT \frac{\delta V_{oc}}{\delta T} \tag{2.14}$$

2.1.1 Deriving the number of cells in the battery pack

When modelling an entire battery pack, as opposed to a single lithium-ion battery cell, it is essential to determine the number of cells required in series and parallel configurations. Once the cell arrangement is established, the battery pack can be modelled by applying an EECM to each individual cell. The number of cells in series is dictated by the

DOI: 10.13009/EUCASS2025-134

required output voltage of the battery pack and can be calculated using equation (2.15)However, series connections between cells also introduce resistance, leading to potential voltage drops. In this study, the assumption is made that the resistance of these connections is negligible compared to the internal resistance of the battery, as it is an order of magnitude smaller. The number of cells connected in parallel depends on either the maximum discharge current of a single cell or the total required capacity of the battery pack, and can be calculated using equation (2.16).

$$N_{series} = \frac{V_{pack}}{V_{cell}^{nom}} \tag{2.15}$$

$$N_{parallel} = \max \left| \frac{I_{pack}}{I_{cell}^{max}}, \frac{Q_{pack}}{Q_{cell}} \right| \tag{2.16}$$

2.2 Electric Circuit Parameter Estimation

To utilize an EECM, it is necessary to estimate the electric circuit parameters at various SoC and cell temperatures (T_c). This estimation yields a look-up table for each circuit parameter, enabling linear interpolation of values based on the internal state *(SoC, T_c)* of the battery cell during simulation. The parameter estimation procedure typically commences with the acquisition of experimental data through a hybrid pulse power characterization (HPPC) test. A standard HPPC test involves current pulses of fixed duration and C-rate, as described in [23], [24]. The fixed duration and C-rate allow for the measurement of voltage response at a specific SoC. The pulse duration is determined by the required SoC percentage to be discharged, enabling shorter pulses in highly non-linear regions to achieve improved modelling accuracy. The C-rate of the pulse is selected to approximate typical operating conditions of the battery cell. During the test, the SoC is determined using Coulomb counting, which allows for SoC calculation using equation (2.17).

$$SoC(t) = SoC(t_0) - \frac{\int_{t_0}^{t} I(t)dt}{Q_0} \tag{2.17}$$

The constant Q_0 represents the charge of the cell at time t_0. With the HPPC data available, parameter estimation can be performed by simulating the battery cell using the HPPC current profile and applying a linear regression technique, where the circuit parameters serve as variables, to fit the model's voltage response to the measured HPPC voltage response. In this study, this process was implemented using the Simulink Parameter Estimator application [41] in MATLAB. The regression method employed was non-linear least squares regression, utilizing the gradient-based trust-region reflective optimization algorithm. The bounds on the time constant τ_n was selected such that the RC-pairs would model the dynamics from faster to slower based on the RC-pair number. However, it is essential to note that the parameter estimation procedure described above does not capture temperature dependence. To incorporate this dependency into the EECM circuit parameter tables, the procedure can be repeated at various temperature levels.

2.3 Experimental Setup

An experimental campaign was carried out to acquire the HPPC test data required for circuit parameter estimation of the Samsung INR18650-33G battery cells. The experimental setup was capable of applying a current profile to the battery cell and logging its voltage response while controlling the cell temperature. The experimental setup used in this work to collect this data is illustrated in *Figure 7* and *Figure 8*. A CADEX battery analyser was utilized as a current source and temperature logger, enabling current pulses of up to 2C to be drawn from the battery cell, with temperature measurements logged at a resolution of 1 K using a surface temperature sensor. The voltage response of the battery cells was measured using a Fluke multi-meter. Both the CADEX battery analyser and multi-meter were connected to a laptop, facilitating data logging and storage. To maintain a consistent ambient and cell temperature, the entire setup was housed within a thermal chamber.

DOI: 10.13009/EUCASS2025-134

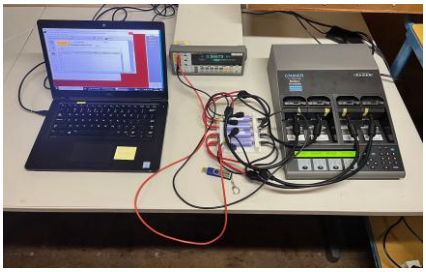

Figure 7: The experimental setup used to test the battery cells

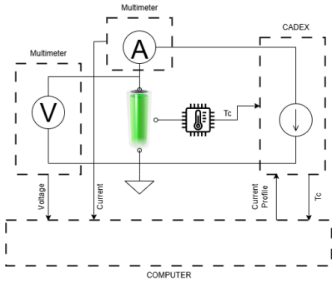

Figure 8: Diagram of the experimental setup

Three different types of tests were performed. Initially, each new battery cell underwent a break-in procedure consisting of 5 full charge-discharge cycles to ensure proper operation and stabilize its behaviour. Then, a constant-current-charge-and-discharge test (CCDT) was conducted at a rate of 1C to extract the constant current charge and discharge characteristics of the battery cell. Next, four HPPC tests were performed at temperatures of 0, 10, 25, and 45 degrees Celsius. Additionally, an attempt was made to obtain the necessary data for determining the entropic coefficients through an entropic coefficient test (ECT). To minimize variability and ensure consistency across tests, a new battery cell was used for each test type, thereby eliminating the influence of battery age (SoH) between tests.

2.4 Lumped Parameter Thermal Network Model

In this work, the thermal interaction between the battery cells, coolant, and ambient conditions has been modelled using a LPTN model. A LPTN consists of nodes with lumped thermal capacitance, where one or multiple battery cells are aggregated into a single node with a uniform (average) temperature. Increasing the number of nodes in the network enhances model accuracy but also increases complexity. Each node has a thermal mass, which can be calculated by summing the thermal capacities of the elements lumped together, as expressed in equation (2.18) where C is the total thermal mass (in J/K), $c_{p,i}$ is the specific heat capacity of each component (in J/kgK), and m_i is the mass of each component. The battery cells analysed in this work employed a Nickel-Manganese-Cobalt (NMC) chemistry. According to [8], [42], the specific heat capacity of a NMC battery cell was determined using the rule of mixtures to be 1040±43 J/kgK. Although the specific heat of the battery cell was found to vary with the SoC by 2-5%, this variation was deemed negligible, and the specific heat capacity was assumed to remain constant at 1040 J/kgK to reduce model complexity. The assumption of lumping a battery cell into a single thermal node with thermal mass and average temperature is valid only when the Biot number is significantly less than 0.1. If the Biot number exceeds this threshold, it is likely that a strong thermal gradient is present within the battery cell, which would need to be considered in the model.

$$C = \sum_{i=1}^{n} c_{p,i} \cdot m_i \tag{2.18}$$

The interaction between nodes, coolant, and ambient conditions can be modelled by connecting nodes with thermal resistances, whose values depend on the heat transfer mode and geometric arrangement between nodes. This work considers two primary modes of heat transfer: conduction and convection. Although radiation is another means of heat transfer, its effect is deemed negligible compared to conduction and convection due to the relatively low battery cell temperature (<60°C).

Thermal conduction refers to the diffusion of thermal energy within a material or between materials in contact. The heat transfer equation for conduction is given by equation (2.19) where k represents the thermal conductivity of the material [43], A is the heat transfer area [m²], and L is the length of heat transfer [m]. From equation (2.19), the thermal resistance, which opposes heat transfer, can be expressed as in equation (2.20). In a similar manner the heat transfer due to movement of a fluid; convection can be modelled. The convective heat transfer equation, also known as Newton's law of cooling, is given by Equation (2.21) [43]. In this equation, h represents the heat transfer coefficient, which is typically determined using empirical relationships that depend on the type of flow and flow regime. These relationships often involve non-dimensional characterization numbers, such as the Reynolds, Prandtl, and Grasshof numbers. The thermal resistance due to convection can be calculated using Equation (2.22), which provides a quantitative measure of the opposition to heat transfer.

$$\dot{Q}_{cond} = \frac{kA}{L}\Delta T \tag{2.19}$$

DOI: 10.13009/EUCASS2025-134

$$R_{cond} = \frac{L}{kA} \tag{2.20}$$

$$\dot{Q}_{conv} = hA\Delta T \tag{2.21}$$

$$R_{conv} = \frac{1}{hA} \tag{2.22}$$

Upon determining the thermal resistances between nodes, a thermal network can be constructed. By representing thermal interactions as resistances, an analogy can be drawn with electric circuits, thereby enabling the application of Kirchhoff's laws to solve the network model. Utilizing this electrical system analogy, the thermal network is established by connecting each thermal node to its neighbouring nodes, as well as to the coolant and ambient conditions. An exemplary four-node LPTN is depicted in Figure 9, demonstrating the application of this methodology.

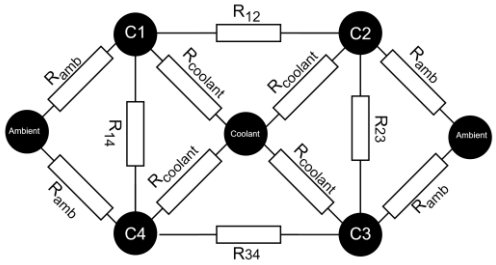

Figure 9: An example of a LPTN for four (cell) nodes

The thermal resistances between nodes are significantly influenced by the geometric arrangement of the cells and the type of thermal management system employed. Ribbon cooling [44] of the cells was assumed in this study (see Figure 10 and Figure 11). To calculate the thermal resistances between the nodes, a geometric parameterization is necessary. The results of this parameterization are illustrated in Figure 10 and Figure 11. The thermal resistance of the cooling ribbon is subsequently calculated using an approach similar to that described in [45], as expressed in equation (2.23). Where t_{ribbon} is the thickness of the ribbon [m], d_{cell} is the battery cell diameter [m], h_{cell} the battery cell height [m] and f_{ribbon} [-] the fraction of the battery cell covered by the ribbon. However, this calculation excludes the thermal resistance associated with convection within the cooling duct. The convective heat transfer resistance - following equation (2.22) - to the coolant was calculated separately, utilizing the Nusselt number and the Gnielinski correlation [46].

$$R_{ribbon,cond} = \frac{t_{ribbon}}{k \cdot \phi \cdot \frac{2\pi}{360} \cdot d_{cell} \cdot h_{cell} \cdot f_{ribbon}} \tag{2.23}$$

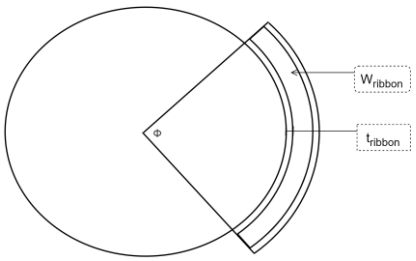

Figure 10: Ribbon cooling parameterization top view

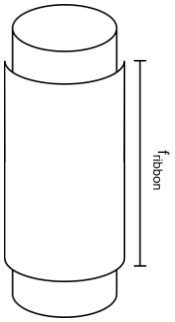

Figure 11: Ribbon cooling parameterization side view

The ambient thermal path (i.e., the thermal interaction between the cell and the ambient environment, apart from the ribbon-cooling) is determined using a method similar to that presented in [45]. The process involves conduction of heat away from the cell walls into the stagnant air within the battery pack, followed by convection of heat from this air to the enclosure walls. The heat is then conducted through these walls by convection (Figure 12). The thermal resistances associated with the thermal paths can be calculated using the general equations for conduction and convection.

DOI: 10.13009/EUCASS2025-134

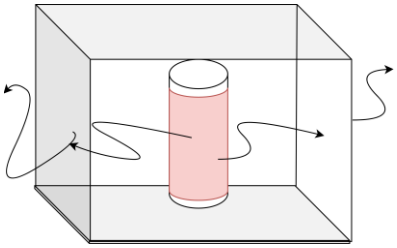

Figure 12: Ambient thermal path

The thermal resistances between the cells can be determined by examining the possible heat transfer pathways between the cells. In a hexagonal cell stacking arrangement with a cooling ribbon between cells, direct conduction between cells is not feasible. As a result, heat transfer between cells can only occur through free convection. However, the heat flux associated with free convection is significantly lower than that of conduction and forced convection. Therefore, it is assumed that the thermal resistance between cells is effectively infinite, and that heat transport occurs primarily via two pathways: the coolant and the ambient.

3 Results & Discussion

This chapter describes the main results that were found in our study. The battery cell experiment and the estimated EECM parameters are presented in section 3.1. After that the voltages predicted by the EECM are compared to additional battery cell test data and to the measured voltages on the Pipistrel aircraft, in section 3.2. Finally, the coupled EECM and thermal model are compared to measured battery cell temperatures, also in section 3.2. This resulted in a validated EECM and LPTN model of the Pipistrel Velis Electro battery.

3.1 Cell Parameterization

Using the experimental setup described in Section 2.3, the necessary data for the Samsung battery cell parameterization was acquired. The resulting constant current charge and discharge curves are shown in Figure *13*. As evident from Figure *13*, the non-linear behaviour of the cell is pronounced at low and high discharge capacities. Furthermore, it is observed that increasing the temperature leads to an increase in battery capacity, as the cut-off voltage[1] is reached at higher discharge capacities.

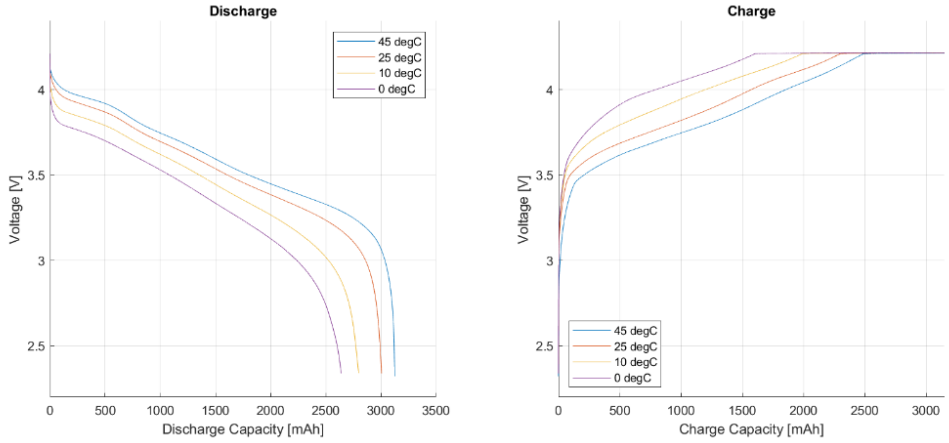

Figure 13: Continuous current charge- and discharge curves for the SAMSUNG INR-18650-33G Cell

The HPPC test yielded four datasets, each corresponding to a different temperature level. The results of the HPPC test at 25°C are presented in Figure 14, which clearly illustrates the dynamic voltage response after each current pulse. However, the cell temperature during the test deviated from the setpoint of 25°C. This can be attributed to the large volume of the thermal chamber relative to the size of the tested battery cell, making it more difficult to control the temperature. Although the cell temperature varied by up to 2°C, this deviation is not expected to have a substantial impact on the estimated circuit parameters.

[1] This the minimal (feasible) voltage. When this value is reached the experiment is ended.

DOI: 10.13009/EUCASS2025-134

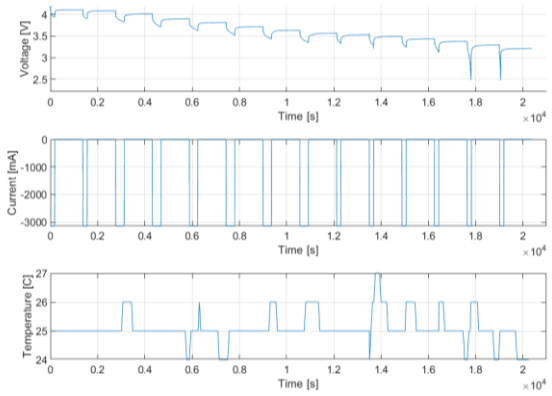

Figure 14 The results of the HPPC from the Samsung INR18650-33G cell at 25˚C

Using the HPPC data, the circuit parameters for the EECMs were estimated for 0-, 1-, 2-, and 3-RC pair configurations, following the methods described in section 2.2. The resulting circuit parameters for a 2-RC pair EECM are presented in Figure 15. As evident from Figure 15, there is a notable increase in the resistance values of the circuit components at low states of charge (SoC) and temperatures, which is consistent with theoretical expectations that the internal resistance of the battery cell increases with decreasing SoC and temperature. Furthermore, the time constants $\tau 1$ and $\tau 2$ reveal that $\tau 1$ is smaller than $\tau 2$, indicating that the faster battery dynamics are captured by RC-1, while the slower dynamics are represented by RC-2.
The effect of the other estimated n-RC EECMs is summarized in the next subsection, in terms of model accuracy.

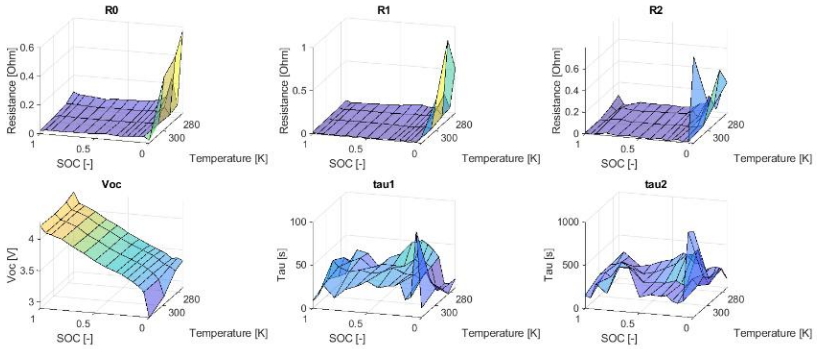

Figure 15:The resulting circuit parameters for a 2-RC pair EECM

3.2 Model Validation

The developed coupled electro-thermal model was validated using both constant current discharge data from the experimental campaign and actual in-flight data logged by the Battery Management System (BMS) aboard the Pipistrel Aircraft. The validation, by comparing the 2-RC model prediction results to the data of constant current discharge test at a cell temperature of 10°C, is presented in Figure 16. As shown in Figure 16, the model exhibits good agreement with the data, particularly at low discharge capacities. However, at higher discharge capacities, an increase in modelling error (residual) is observed, which can likely be attributed to the model's limited ability to capture the highly non-linear behaviour of the battery cell at high discharge rates. Similar validation results were obtained for the other three temperatures (0 °C , 25 °C and 45°C).

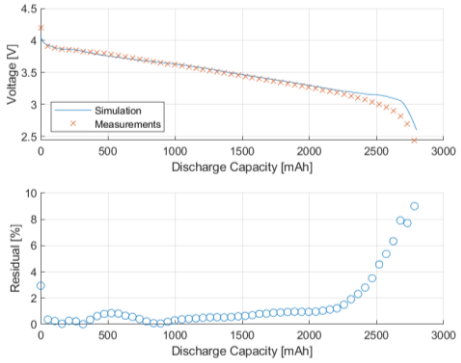

Figure 16:Validation of the 2-RC EECM with 1C continuous discharge current data at 10˚C

DOI: 10.13009/EUCASS2025-134

In addition to the constant discharge current validation, a validation using flight data was performed to assess both the electrical and thermal accuracy of the developed model. The flight profile used for validation is shown in Figure 17 and Figure 18. The test flight was conducted at Rotterdam The Hague Airport, which is located below sea level, thus explaining the negative starting altitude. The flight consisted of a typical take-off, climb, cruise, and descent, followed by four go-around procedures, resulting in the four peaks observed after the descent phase.
The electrical validation results for the 2-RC EECM are shown in Figure 19. For the electric validation the first 500 seconds of the flight profile have been removed as there was no current drawn from the battery until this point. It is evident that, when properly parameterized, the model accurately simulates the battery voltage response, with a maximum residual error of less than 2%. A comparative analysis was conducted among 0-, 1-, 2-, and 3-RC pair models (see Table 3). This analysis involved simulating the same flight profile and recording the residual mean square error (RMSE) and maximum error for each model. As shown in Table 3, the 2-RC EECM strikes a balance between RMSE and maximum error, outperforming the other models in this regard. However, it is notable that the differences between the models are relatively small, which raises questions about whether the increased complexity of the 2-RC model justifies its marginal improvement in modelling accuracy over the simpler 1-RC model.

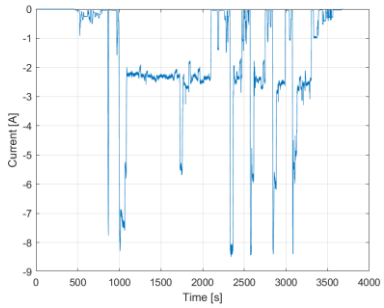

Figure 17: The current profile of the test flight

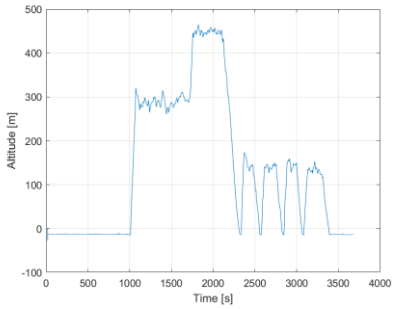

Figure 18:The altitude data of the test flight

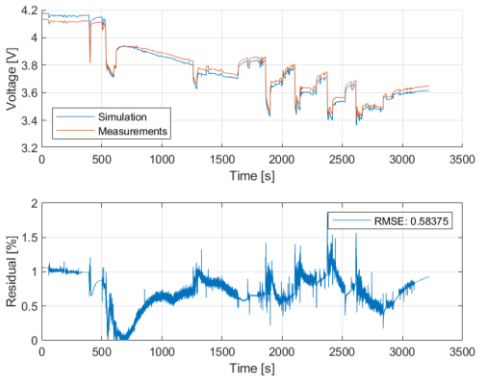

Figure 19: Simulated and measured voltage for flight test data using a 2RC EECM

Table 1: Comparison between xRC on RMSE and Max Error for flight profile simulation

EECM	RMSE [%]	Max Error [%]
0-RC	2.04	9.01
1-RC	0.53	2.39
2-RC	0.58	1.86
3-RC	1.07	2.18

The coupled electro-thermal model was validated by comparing the simulated maximum battery pack [2]temperature with the measured maximum pack temperature during the test flight, as shown in Figure 20. The results indicate that, using the configured EECM and LPTN, the model accurately simulates the battery pack temperature. Although the BMS logged temperatures with a relatively coarse resolution of 1 K, the comparison reveals that the model captures the minimum, maximum, and trend of the measured temperature. Figure 20 also illustrates that the battery cell

[2] maximum battery cell temperature measured in the battery pack

DOI: 10.13009/EUCASS2025-134

temperature increases most during periods of high current, corresponding to high power settings typically encountered during take-off conditions and go-around attempts. Specifically, these events occurred at 500 s and 2250 s, and Figure 20 shows a clear rise in battery pack temperature at these time steps.

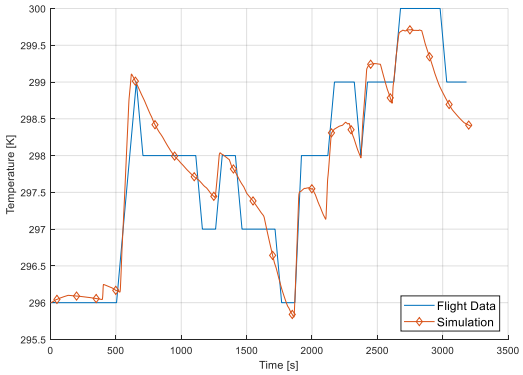

Figure 20:A comparison between the simulated maximum battery pack temperature and the corresponding data from the BMS

4 Conclusion

In this study, a coupled electro-thermal model to simulate the thermal behaviour of lithium-ion battery packs for electric aircraft has been developed and validated with flight data of the Pipistrel Velis Electro. The model integrates an EECM with a LPTN to simulate both voltage output and heat generation, as well as the resulting temperature distribution within the battery pack.

A key contribution of this work lies in the accurate prediction of battery cell (and pack) temperatures under real-world flight conditions. The LPTN model was developed using calculated thermal resistances between battery cells, coolant ribbons, and ambient environment, based on the geometric configuration of the Velis Electro battery pack. The EECM was developed using parameter estimations from dedicated cell level experiments.

By combining the LPTN with the heat generation predicted using the EECM—including both irreversible (Joule) and reversible (entropic) heating—the model successfully predicted the voltage response and the thermal dynamics of the battery system. Validation against flight test data showed that the model accurately captured both the maximum pack temperatures and the transient temperature evolution, with deviations well within 1 K of the logged BMS data.

These results confirm the model capability to simulate not only electrical behaviour but also thermal performance under varying load and environmental conditions. The work underscores the importance of integrated electro-thermal modelling for ensuring the safety, efficiency, and longevity of battery systems in electric aviation. Future work may include dynamic modelling of thermal runaway risk, long-term ageing effects, and adaptation to larger battery configurations (for larger aircraft) or alternative chemistries. Additionally minimize temperature deviations in future experiments, it is recommended to use either a smaller thermal chamber or a more direct thermal control solution.

List of symbols

Symbol	Description	Unit
V	Terminal voltage of the battery cell	V
I	Current drawn from the battery (positive: charging, negative: discharging)	A
R_0, R_n	Internal resistances in EECM (n = 1, 2, 3…)	Ω
C_n	Capacitances in EECM	F
τ_n	Time constant of RC pair, $\tau_n = R_nC_n$	s
V_{oc}	Open-circuit voltage	V
SoC	State of Charge	% or Fraction
SoH	State of Health	% or Fraction
Tc	Cell temperature	K or °C
ΔS	Change in entropy	J/(mol·K)
$\dot{Q}_{irr}$	Irreversible (Joule) heat generation	W
$\dot{Q}_{rev}$	Reversible (entropic) heat generation	W
n	Number of electrons in redox reaction (for Li-ion, n = 1)	–
F	Faraday constant (96,485)	C/mol
C	Thermal capacitance (LPTN)	J/K
R_{th}	Thermal resistance	K/W

DOI: 10.13009/EUCASS2025-134

h	Convective heat transfer coefficient	W/(m²·K)
k	Thermal conductivity	W/(m·K)
A	Heat transfer area	m²
L	Characteristic length for conduction	m
Bi	Biot number	–

Abbreviations

Abbreviation	Full Term
BE	Battery Electric
BMS	Battery Management System
EECM	Electric Equivalent Circuit Model
LPTN	Lumped Parameter Thermal Network
OCV	Open-Circuit Voltage
HPPC	Hybrid Pulse Power Characterization
CCDT	Constant Current Charge and Discharge Test
NMC	Nickel-Manganese-Cobalt (cathode chemistry)
RC	Resistor-Capacitor
SoC	State of Charge
SoH	State of Health
DFN	Doyle-Fuller-Newman (electrochemical model)
ECT	Entropic Coefficient Test
RMSE	Root Mean Square Error

References

[1] B. Owen, D. S. Lee, and L. Lim, 'Flying into the Future: Aviation Emissions Scenarios to 2050', *Environ. Sci. Technol.*, vol. 44, no. 7, pp. 2255–2260, Apr. 2010, doi: 10.1021/es902530z.

[2] R. E. Wolleswinkel, R. De Vries, M. Hoogreef, and R. Vos, 'A New Perspective on Battery-Electric Aviation, Part I: Reassessment of Achievable Range', in *AIAA SCITECH 2024 Forum*, Orlando, FL: American Institute of Aeronautics and Astronautics, Jan. 2024. doi: 10.2514/6.2024-1489.

[3] G. Zilliac, J. V. Bowles, R. K. Fong, M. Schuh, D. Pham, and V. Kuptsov, 'Feasibility Study of an All-Electric 150 Passenger Aircraft', in *AIAA AVIATION FORUM AND ASCEND 2024*, Las Vegas, Nevada: American Institute of Aeronautics and Astronautics, Jul. 2024. doi: 10.2514/6.2024-3872.

[4] H. D. Kim, A. T. Perry, and P. J. Ansell, 'A Review of Distributed Electric Propulsion Concepts for Air Vehicle Technology', in *2018 AIAA/IEEE Electric Aircraft Technologies Symposium*, Cincinnati, Ohio: American Institute of Aeronautics and Astronautics, Jul. 2018. doi: 10.2514/6.2018-4998.

[5] Pipistrel Vertical Solutions, *Pilot's Operating Handbook Velis Electro*, 2nd ed. Slovenia: Pipistrel Vertical Solutions, 2022.

[6] M. Alkhedher, A. B. Al Tahhan, J. Yousaf, M. Ghazal, R. Shahbazian-Yassar, and M. Ramadan, 'Electrochemical and thermal modeling of lithium-ion batteries: A review of coupled approaches for improved thermal performance and safety lithium-ion batteries', *J. Energy Storage*, vol. 86, p. 111172, May 2024, doi: 10.1016/j.est.2024.111172.

[7] Y. Ye, Y. Shi, N. Cai, J. Lee, and X. He, 'Electro-thermal modeling and experimental validation for lithium ion battery', *J. Power Sources*, vol. 199, pp. 227–238, Feb. 2012, doi: 10.1016/j.jpowsour.2011.10.027.

[8] M. V. Morganti, S. Longo, M. Tirovic, C.-Y. Blaise, and G. Forostovsky, 'Multi-Scale, Electro-Thermal Model of NMC Battery Cell', *IEEE Trans. Veh. Technol.*, vol. 68, no. 11, pp. 10594–10606, Nov. 2019, doi: 10.1109/TVT.2019.2943052.

[9] M. Doyle, T. F. Fuller, and J. Newman, 'Modeling of Galvanostatic Charge and Discharge of the Lithium/Polymer/Insertion Cell', *J. Electrochem. Soc.*, vol. 140, no. 6, pp. 1526–1533, Jun. 1993, doi: 10.1149/1.2221597.

[10] N. Chaturvedi, K. Reinhardt, J. Christensen, J. Ahmed, and A. Kojic, 'Algorithms for Advanced Battery-Management Systems', *IEEE Control Syst.*, vol. 30, no. 3, pp. 49–68, Jun. 2010, doi: 10.1109/MCS.2010.936293.

[11] Y. Li, Z. Wei, C. Xie, and D. M. Vilathgamuwa, 'Physics-Based Model Predictive Control for Power Capability Estimation of Lithium-Ion Batteries', *IEEE Trans. Ind. Inform.*, vol. 19, no. 11, pp. 10763–10774, Nov. 2023, doi: 10.1109/tii.2022.3233676.

DOI: 10.13009/EUCASS2025-134

[12] K. Liu *et al.*, 'Electrochemical modeling and parameterization towards control-oriented management of lithium-ion batteries', *Control Eng. Pract.*, vol. 124, p. 105176, Jul. 2022, doi: 10.1016/j.conengprac.2022.105176.

[13] J. Zhou, B. Xing, and C. Wang, 'A review of lithium ion batteries electrochemical models for electric vehicles', *E3S Web Conf.*, vol. 185, p. 04001, 2020, doi: 10.1051/e3sconf/202018504001.

[14] M. Martí-Florences, A. Cecilia, and R. Costa-Castelló, 'Modelling and Estimation in Lithium-Ion Batteries: A Literature Review', *Energies*, vol. 16, no. 19, p. 6846, Sep. 2023, doi: 10.3390/en16196846.

[15] V. Lucaferri, M. Quercio, A. Laudani, and F. Riganti Fulginei, 'A Review on Battery Model-Based and Data-Driven Methods for Battery Management Systems', *Energies*, vol. 16, no. 23, p. 7807, Nov. 2023, doi: 10.3390/en16237807.

[16] M. A. Abu-Seif, A. S. Abdel-Khalik, M. S. Hamad, E. Hamdan, and N. A. Elmalhy, 'Data-Driven modeling for Li-ion battery using dynamic mode decomposition', *Alex. Eng. J.*, vol. 61, no. 12, pp. 11277–11290, Dec. 2022, doi: 10.1016/j.aej.2022.04.037.

[17] R. Di Fonso, C. Cecati, R. Teodorescu, D.-I. Stroe, and P. Bharadwaj, 'Data-driven Modeling of Li-ion Battery based on the Manufacturer Specifications and Laboratory Measurements', in *2022 IEEE International Conference on Power Electronics, Drives and Energy Systems (PEDES)*, Jaipur, India: IEEE, Dec. 2022, pp. 1–6. doi: 10.1109/pedes56012.2022.10080375.

[18] E. D. Silva-Vera, J. E. Valdez-Resendiz, G. Escobar, D. Guillen, J. C. Rosas-Caro, and J. M. Sosa, 'Data-Driven Modeling and Open-Circuit Voltage Estimation of Lithium-Ion Batteries', *Mathematics*, vol. 12, no. 18, p. 2880, Sep. 2024, doi: 10.3390/math12182880.

[19] R. R. Thakkar, 'Electrical Equivalent Circuit Models of Lithium-ion Battery', in *Management and Applications of Energy Storage Devices*, K. E. Okedu, Ed., IntechOpen, 2022. doi: 10.5772/intechopen.99851.

[20] L. Zhang, H. Peng, Z. Ning, Z. Mu, and C. Sun, 'Comparative Research on RC Equivalent Circuit Models for Lithium-Ion Batteries of Electric Vehicles', *Appl. Sci.*, vol. 7, no. 10, p. 1002, Sep. 2017, doi: 10.3390/app7101002.

[21] M. Lagnoni, C. Scarpelli, G. Lutzemberger, and A. Bertei, 'Critical comparison of equivalent circuit and physics-based models for lithium-ion batteries: A graphite/lithium-iron-phosphate case study', *J. Energy Storage*, vol. 94, p. 112326, Jul. 2024, doi: 10.1016/j.est.2024.112326.

[22] M.-K. Tran, A. DaCosta, A. Mevawalla, S. Panchal, and M. Fowler, 'Comparative Study of Equivalent Circuit Models Performance in Four Common Lithium-Ion Batteries: LFP, NMC, LMO, NCA', *Batteries*, vol. 7, no. 3, p. 51, Jul. 2021, doi: 10.3390/batteries7030051.

[23] R. Jackey, M. Saginaw, P. Sanghvi, J. Gazzarri, T. Huria, and M. Ceraolo, 'Battery Model Parameter Estimation Using a Layered Technique: An Example Using a Lithium Iron Phosphate Cell', presented at the SAE 2013 World Congress & Exhibition, Apr. 2013, pp. 2013-01–1547. doi: 10.4271/2013-01-1547.

[24] A. Najafi and M. Masih-Tehrani, 'Hybrid adaptive battery parameter estimation approach for equivalent circuit model toolbox', *SoftwareX*, vol. 24, p. 101534, Dec. 2023, doi: 10.1016/j.softx.2023.101534.

[25] W. Wu, S. Wang, W. Wu, K. Chen, S. Hong, and Y. Lai, 'A critical review of battery thermal performance and liquid based battery thermal management', *Energy Convers. Manag.*, vol. 182, pp. 262–281, Feb. 2019, doi: 10.1016/j.enconman.2018.12.051.

[26] G. Karimi and X. Li, 'Thermal management of lithium-ion batteries for electric vehicles: Thermal management of Li-ion battery packs', *Int. J. Energy Res.*, vol. 37, no. 1, pp. 13–24, Jan. 2013, doi: 10.1002/er.1956.

[27] Z. Pan, W. Li, and Y. Xia, 'Experiments and 3D detailed modeling for a pouch battery cell under impact loading', *J. Energy Storage*, vol. 27, p. 101016, Feb. 2020, doi: 10.1016/j.est.2019.101016.

[28] C. Zhang, K. Li, and J. Deng, 'Real-time estimation of battery internal temperature based on a simplified thermoelectric model', *J. Power Sources*, vol. 302, pp. 146–154, Jan. 2016, doi: 10.1016/j.jpowsour.2015.10.052.

[29] W. Allafi *et al.*, 'A lumped thermal model of lithium-ion battery cells considering radiative heat transfer', *Appl. Therm. Eng.*, vol. 143, pp. 472–481, Oct. 2018, doi: 10.1016/j.applthermaleng.2018.07.105.

[30] H. Dai, L. Zhu, J. Zhu, X. Wei, and Z. Sun, 'Adaptive Kalman filtering based internal temperature estimation with an equivalent electrical network thermal model for hard-cased batteries', *J. Power Sources*, vol. 293, pp. 351–365, Oct. 2015, doi: 10.1016/j.jpowsour.2015.05.087.

[31] G. Guo, B. Long, B. Cheng, S. Zhou, P. Xu, and B. Cao, 'Three-dimensional thermal finite element modeling of lithium-ion battery in thermal abuse application', *J. Power Sources*, vol. 195, no. 8, pp. 2393–2398, Apr. 2010, doi: 10.1016/j.jpowsour.2009.10.090.

[32] Y. Li, Z. Zhou, and W.-T. Wu, 'Three-dimensional thermal modeling of Li-ion battery cell and 50 V Li-ion battery pack cooled by mini-channel cold plate', *Appl. Therm. Eng.*, vol. 147, pp. 829–840, Jan. 2019, doi: 10.1016/j.applthermaleng.2018.11.009.

DOI: 10.13009/EUCASS2025-134

[33] A. Smyshlyaev, M. Krstic, N. Chaturvedi, J. Ahmed, and A. Kojic, 'PDE model for thermal dynamics of a large Li-ion battery pack', in *Proceedings of the 2011 American Control Conference*, San Francisco, CA: IEEE, Jun. 2011, pp. 959–964. doi: 10.1109/acc.2011.5991584.

[34] X. Cui *et al.*, 'Optimization of the lumped parameter thermal model for hard-cased li-ion batteries', *J. Energy Storage*, vol. 32, p. 101758, Dec. 2020, doi: 10.1016/j.est.2020.101758.

[35] I. Arasaratnam, J. Tjong, R. Ahmed, M. El-Sayed, and S. Habibi, 'Adaptive temperature monitoring for battery thermal management', in *2013 IEEE Transportation Electrification Conference and Expo (ITEC)*, Metro Detroit, MI, USA: IEEE, Jun. 2013, pp. 1–6. doi: 10.1109/itec.2013.6574504.

[36] Samsung SDI, 'Specification of Product for Lithium-ion rechargeable cell Model name: INR18650-33G'. Samsung SDI, May 28, 2014. [Online]. Available: https://www.dnkpower.com/wp-content/uploads/2022/08/INR-18650-33G.pdf

[37] R. Zhang *et al.*, 'A Study on the Open Circuit Voltage and State of Charge Characterization of High Capacity Lithium-Ion Battery Under Different Temperature', *Energies*, vol. 11, no. 9, p. 2408, Sep. 2018, doi: 10.3390/en11092408.

[38] M. Dürr, A. Cruden, S. Gair, and J. R. McDonald, 'Dynamic model of a lead acid battery for use in a domestic fuel cell system', *J. Power Sources*, vol. 161, no. 2, pp. 1400–1411, Oct. 2006, doi: 10.1016/j.jpowsour.2005.12.075.

[39] H. He, R. Xiong, H. Guo, and S. Li, 'Comparison study on the battery models used for the energy management of batteries in electric vehicles', *Energy Convers. Manag.*, vol. 64, pp. 113–121, Dec. 2012, doi: 10.1016/j.enconman.2012.04.014.

[40] L. B. Diaz, A. Hales, M. W. Marzook, Y. Patel, and G. Offer, 'Measuring Irreversible Heat Generation in Lithium-Ion Batteries: An Experimental Methodology', *J. Electrochem. Soc.*, vol. 169, no. 3, p. 030523, Mar. 2022, doi: 10.1149/1945-7111/ac5ada.

[41] Mathworks, 'Parameter Estimation', Parameter Estimation. [Online]. Available: https://nl.mathworks.com/discovery/parameter-estimation.html

[42] A. Loges, S. Herberger, P. Seegert, and T. Wetzel, 'A study on specific heat capacities of Li-ion cell components and their influence on thermal management', *J. Power Sources*, vol. 336, pp. 341–350, Dec. 2016, doi: 10.1016/j.jpowsour.2016.10.049.

[43] K&K Associates, *Thermal Network Modeling Handbook*, 97th ed. Westminster.

[44] P. Fu, L. Zhao, X. Wang, J. Sun, and Z. Xin, 'A Review of Cooling Technologies in Lithium-Ion Power Battery Thermal Management Systems for New Energy Vehicles', *Processes*, vol. 11, no. 12, p. 3450, Dec. 2023, doi: 10.3390/pr11123450.

[45] J. Zhu, H. Zhang, G. Wu, S. Zhu, and W. Liu, 'Thermal performance of cylindrical battery module with both axial and radial thermal paths: Numerical simulation and thermal resistance network analysis', *J. Energy Storage*, vol. 49, p. 104197, May 2022, doi: 10.1016/j.est.2022.104197.

[46] S. M. Ammar and C. W. Park, 'Validation of the Gnielinski correlation for evaluation of heat transfer coefficient of enhanced tubes by non-linear regression model: An experimental study of absorption refrigeration system', *Int. Commun. Heat Mass Transf.*, vol. 118, p. 104819, Nov. 2020, doi: 10.1016/j.icheatmasstransfer.2020.104819.